


**Please cite the Published Version**

Hellstern, TR, Kibsgaard, J, Tsai, C, Palm, DW, King, LA , Abild-Pedersen, F and Jaramillo, TF (2017) Investigating Catalyst–Support Interactions To Improve the Hydrogen Evolution Reaction Activity of Thiomolybdate [Mo<sub>3</sub>S<sub>13</sub>]<sup>2–</sup> Nanoclusters. ACS Catalysis, 7 (10). pp. 7126-7130. ISSN 2155-5435

**DOI:** <https://doi.org/10.1021/acscatal.7b02133>

**Publisher:** American Chemical Society (ACS)

**Version:** Accepted Version

**Downloaded from:** <https://e-space.mmu.ac.uk/624307/>

**Usage rights:**  In Copyright

**Additional Information:** This is an Author Accepted Manuscript of an article published in ACS Catalysis.

**Enquiries:**

If you have questions about this document, contact [openresearch@mmu.ac.uk](mailto:openresearch@mmu.ac.uk). Please include the URL of the record in e-space. If you believe that your, or a third party's rights have been compromised through this document please see our Take Down policy (available from <https://www.mmu.ac.uk/library/using-the-library/policies-and-guidelines>)

# Investigating Catalyst-Support Interactions to Improve the Hydrogen Evolution Reaction Activity of Thiomolybdate $[\text{Mo}_3\text{S}_{13}]^{2-}$ Nanoclusters

Thomas R. Hellstern<sup>‡</sup>, Jakob Kibsgaard<sup>‡</sup>, Charlie Tsai, David W. Palm, Laurie A. King, Frank Abild-Pedersen, Thomas F. Jaramillo\*

T.R. Hellstern, J. Kibsgaard, C. Tsai, David W. Palm, L.A. King, Prof. T.F. Jaramillo

Department of Chemical Engineering, Stanford University  
443 Via Ortega, Stanford, California 94305, United States

J. Kibsgaard, Frank Abild-Pedersen, Prof. T.F. Jaramillo

SUNCAT Center for Interface Science and Catalysis, SLAC National Accelerator Laboratory  
2575 Sand Hill Road, Menlo Park, California, 94025, United States

J. Kibsgaard

Department of Physics, Technical University of Denmark, DK-2800 Kongens Lyngby, Denmark

**KEYWORDS:** *hydrogen evolution reaction, molybdenum sulfide, electrochemistry, renewable energy, catalyst-support interactions*

---

**ABSTRACT:** Molybdenum sulfides have been identified as promising materials for catalyzing the hydrogen evolution reaction (HER) in acid, with active edge sites that exhibit some of the highest turnover frequencies among non-precious metal catalysts. The thiomolybdate  $[\text{Mo}_3\text{S}_{13}]^{2-}$  nanocluster catalyst contains a structural motif that resembles the active site of  $\text{MoS}_2$  and has been reported to be among the most active forms of molybdenum sulfide. Herein, we improve the activity of the  $[\text{Mo}_3\text{S}_{13}]^{2-}$  catalysts through catalyst-support interactions. We synthesize  $[\text{Mo}_3\text{S}_{13}]^{2-}$  on gold, silver, glassy carbon, and copper supports to demonstrate the ability to tune the hydrogen binding energy of  $[\text{Mo}_3\text{S}_{13}]^{2-}$  using catalyst-support electronic interactions and optimize HER activity.

---

Hydrogen is an extremely important industrial chemical, which is produced on a scale of 65 million metric tons per year and used primarily for ammonia synthesis and hydrocarbon upgrading.<sup>1, 2</sup> Currently, steam reforming of natural gas, which produces  $\text{CO}_2$  as a byproduct, is the major process used to generate hydrogen. However, more sustainable methods, such as electrochemical and photoelectrochemical water splitting have the potential to substantially reduce the greenhouse gas emissions associated with hydrogen production.<sup>3-6</sup>

The hydrogen evolution reaction ( $2\text{H}^+ + 2\text{e}^- \rightarrow \text{H}_2$ ) constitutes half of the overall water splitting reaction. Catalysts are required to reduce the overpotential to drive the HER in water splitting devices and achieve high energetic efficiencies. Currently, Pt catalysts are the most active materials for

catalyzing HER, requiring the lowest overpotentials to run at high reaction rates.<sup>7, 8</sup> However, Pt is an expensive precious metal and may suffer from scalability issues as the demand for hydrogen increases.<sup>9</sup> A key challenge in building scalable, cost effective, and efficient water splitting devices is the development of non-precious catalyst formulations that approach the activity of Pt.

Numerous studies have proposed non-precious metal alternatives to platinum, the most active of which are nickel-based electrocatalysts such as Ni, NiMo and NiFe in basic conditions,<sup>7, 10, 11</sup> and transition metal sulfides, phosphides, selenides, borides, carbides, and nitrides, in acidic conditions.<sup>8, 12-21</sup> Molybdenum sulfide is one of the most active, earth abundant catalysts with a turnover frequency (TOF), that is the number of hydrogen molecules produced per active site per second, amongst the highest reported

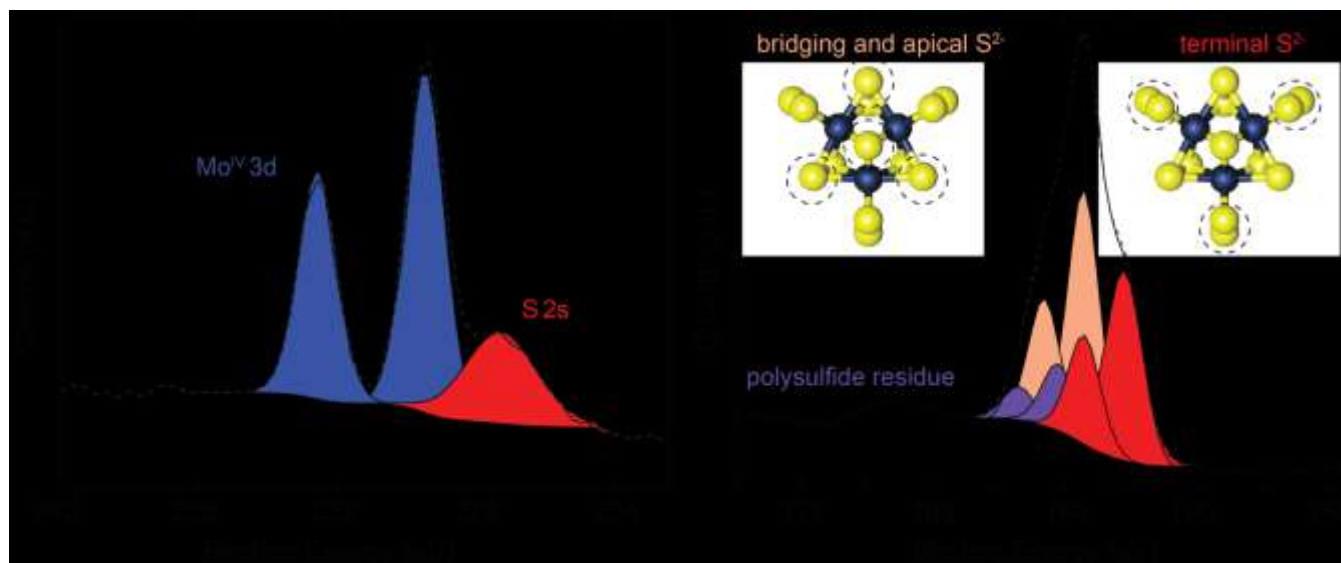


Figure 1. XPS spectra of  $[\text{Mo}_3\text{S}_{13}]^{2-}$  clusters deposited on a Au support. **a.** Mo 3d spectrum shows peaks corresponding to Mo in 4+ oxidation state (blue) and S 2s (red). **b.** S 2p spectrum is deconvoluted into three sets of doublets corresponding to (1) terminal  $\text{S}_2^{2-}$  (red), (2) bridging and apical  $\text{S}_2^{2-}$  and  $\text{S}^{2-}$  (tan), and (3) polysulfide residue (purple)

for a non-precious material.<sup>22, 23</sup> However,  $\text{MoS}_2$  is highly anisotropic, with only its edge sites active for HER, necessitating the engineering of electrodes that expose a high density of active edge sites or the designing of chemically or structurally similar analogues to the  $\text{MoS}_2$  edge. To date, highly nanostructured  $\text{MoS}_2$ ,<sup>23, 24</sup> amorphous  $\text{MoS}_x$ ,<sup>25, 26</sup> different  $\text{MoS}_2$  crystal phases,<sup>27, 28</sup> have all been used to create highly efficient HER electrodes. Small molecules have also been employed as highly active HER catalysts.<sup>29-31</sup> One particular example, thiomolybdate  $[\text{Mo}_3\text{S}_{13}]^{2-}$  contains a structural motif that resembles the active site of  $\text{MoS}_2$  and has been reported to be among the most active forms of molybdenum sulfide.<sup>22, 31</sup>

It has been shown that an optimal catalyst for HER requires a differential hydrogen binding energy ( $\Delta G_{\text{H}}$ ) of 0 eV,<sup>32, 33</sup> which is expected to lead to the highest rates of reaction. Accordingly,  $\text{MoS}_2$  and other pure and alloyed transition metals and transition metal compounds have all been found to have near-zero  $\Delta G_{\text{H}}$ .<sup>33-36</sup> In order to tune the  $\Delta G_{\text{H}}$  of  $\text{MoS}_2$  catalysts to improve their already excellent intrinsic activity, multiple strategies including active site doping and inducing strain have been previously employed.<sup>37-40</sup> In this study, we use catalyst-substrate electronic interactions, which has been proposed through DFT calculations, as an effective strategy for tuning the  $\Delta G_{\text{H}}$  of molybdenum sulfide catalysts and thereby optimize their intrinsic activity.<sup>41</sup>

Herein we demonstrate that HER activity can be improved via interactions between a metal support and  $[\text{Mo}_3\text{S}_{13}]^{2-}$  cluster catalysts. We deposited thin layers (approx.  $1 \times 10^{15}$  clusters  $\text{cm}^{-2}$ ) of thiomolybdate  $[\text{Mo}_3\text{S}_{13}]^{2-}$  nanoclusters on gold, silver, copper, and glassy carbon supports and measured their HER activity. In this work, we show that the HER

activity of the  $[\text{Mo}_3\text{S}_{13}]^{2-}$  clusters changes as a function of the support material. We provide insights into these effects by means of density functional theory (DFT), in which we calculate the change in the hydrogen binding energy for each  $[\text{Mo}_3\text{S}_{13}]^{2-}$  catalyst as a function of support. Our experiments and calculations explain the observed correlation of HER activity for each catalyst-support system with the calculated  $\Delta G_{\text{H}}$ , finding that  $[\text{Mo}_3\text{S}_{13}]^{2-}/\text{Au}$  was the most efficient electrode. Broadly, we demonstrate catalyst-support interactions as an important tool to improve the activity of HER catalysts.

#### Synthesis of $[\text{Mo}_3\text{S}_{13}]^{2-}$ clusters and electrode preparation

The catalyst precursor,  $(\text{NH}_4)_2\text{Mo}_3\text{S}_{13} \cdot \text{H}_2\text{O}$ , was synthesized following a previously reported procedure (see Supporting Information).<sup>31, 42</sup> X-ray diffraction, shown in Fig. S1, was performed to confirm the correct  $[\text{Mo}_3\text{S}_{13}]^{2-}$  crystal structure. The catalyst-support combinations were prepared by sputtering 10 nm of Ti followed by 50 nm of Cu, Au or Ag onto glassy carbon rotating disk electrodes. The  $[\text{Mo}_3\text{S}_{13}]^{2-}$  clusters were deposited onto the substrates by spray coating from a 1 mM methanol solution. The catalyst loading was kept low (approx.  $10^{15}$  clusters  $\text{cm}^{-2}$ ) to ensure proximity of catalyst to the support which is necessary to observe the full impact of support effects on catalysis.

#### Chemical characterization by X-ray Photoelectron Spectroscopy

The chemical state of the  $[\text{Mo}_3\text{S}_{13}]^{2-}$  clusters was investigated using X-ray photoelectron spectroscopy (XPS) as shown in Fig. 1. The molybdenum 3d region shows the presence of a doublet corresponding to Mo in a 4+

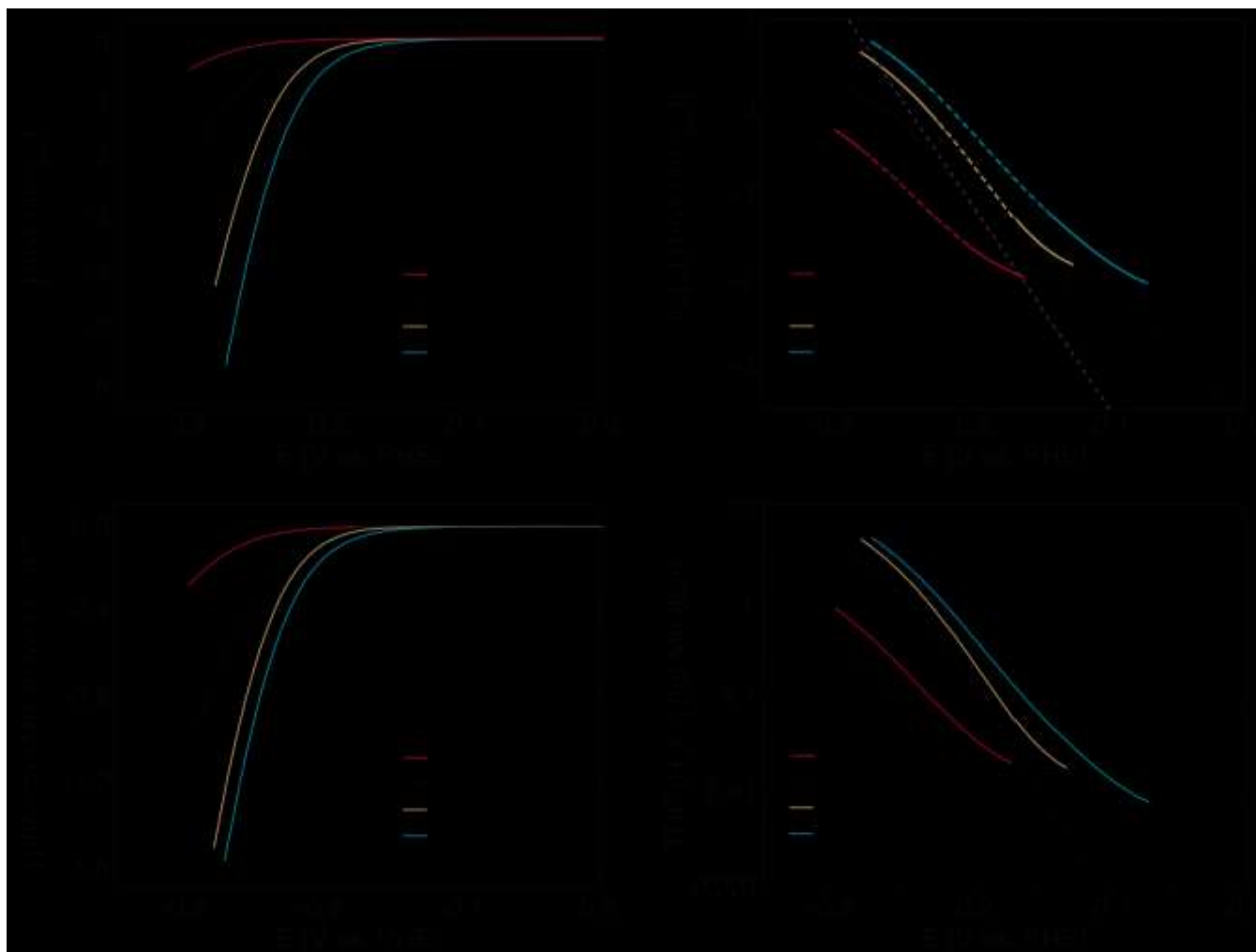


Figure 2. Characterization of the electrochemical activity of each catalyst-support system; [Mo<sub>3</sub>S<sub>13</sub>]<sup>2-</sup> on gold (blue), silver (yellow), glassy carbon (black), and copper (red). **a.** Geometric activity of electrodes. **b.** Tafel analysis of polarization curves. **c.** Current density of each electrode normalized to mass loading. Mass loadings were determined by ICP-MS and range from  $1.6 \times 10^{15}$  Mo atoms cm<sup>-2</sup> to  $3.6 \times 10^{15}$  Mo atoms cm<sup>-2</sup>. **d.** TOF plot of the [Mo<sub>3</sub>S<sub>13</sub>]<sup>2-</sup> electrodes per Mo atom.

#### Chemical characterization by X-ray Photoelectron Spectroscopy

oxidation state (Mo 3d<sub>5/2</sub> = 229.5 eV, Mo 3d<sub>3/2</sub> = 232.6 eV). A sulfur 2s peak is also present at 227.3 eV with a large full width at half maximum (FWHM) indicating the presence of sulfur in multiple oxidation states. The sulfur 2p region can be deconvoluted into three distinct doublets corresponding to (1) terminal S<sub>2</sub><sup>2-</sup> sulfide ligands which are coordinated to one molybdenum (162.2 eV, 163.4 eV), (2) bridging S<sub>2</sub><sup>2-</sup> sulfide ligands and the apical S<sup>2-</sup> ligand which are coordinated to two or three molybdenums respectively (163.4 eV, 164.6 eV), and (3) residual polysulfide arising from the synthesis of the clusters (164.3 eV, 165.5 eV). Quantification reveals a ratio of ~ 7:6 when comparing the intensity of the bridging and apical sulfur lines to the terminal sulfur line as expected. These results are consistent with previously reported spectra for [Mo<sub>3</sub>S<sub>13</sub>]<sup>2-</sup> and the XPS spectra look the same for all as-deposited samples regardless of support.<sup>42-45</sup> Spectra taken after HER testing are available in Fig. S2 and show that there is a loss of bridging and apical sulfurs compared to terminal sulfurs. Fig. S3 shows an Auger Electron

Spectroscopy (AES) map of the catalyst distribution on the electrode surface.

#### Hydrogen evolution activity

The electrodes were evaluated for HER activity using a three-electrode rotating disk electrode (RDE) electrochemical setup (conditions: H<sub>2</sub>-purged, reversible hydrogen reference electrode (RHE), sweep rate 10 mV s<sup>-1</sup>, 1600 rpm).

A comparison of the geometric catalytic activity of the [Mo<sub>3</sub>S<sub>13</sub>]<sup>2-</sup> clusters supported on gold, silver, glassy carbon (GC), and copper is shown in Fig. 2a. The onset for HER current, defined here as the overpotential required to achieve -0.1 mA cm<sup>-2</sup>, is -0.15 V, -0.18 V, -0.20 V, and -0.24 V for [Mo<sub>3</sub>S<sub>13</sub>]<sup>2-</sup> supported on Au, Ag, GC, and Cu respectively. The HER activity of the bare supports can only account for a very small fraction of the total geometric activity as shown in Fig. S4. [Mo<sub>3</sub>S<sub>13</sub>]<sup>2-</sup>/Au, which has the highest geometric catalytic activity, also has the highest catalyst loading by a factor of ~2, as determined by inductively coupled plasma mass spectrometry (ICP-MS). Catalyst loading for all electrodes is reported in the supporting information. Though the cata-

lysts were deposited on all supports simultaneously, differences in support affinity for the molybdenum sulfide clusters could account for variations in loading. In order to gain insight into changes in mechanisms of catalysis as a function of loading, we performed a Tafel analysis.

Tafel plots of the polarization curves are provided in Fig. 2b. The Tafel slope of a catalyst, which is reported in mV/decade, can help provide mechanistic insight into reaction pathways.<sup>46-49</sup> For instance, for an HER catalyst operating under ideal conditions, it has been suggested that a Tafel slope of 40 mV/decade indicates that it follows a Volmer-Heyrovsky HER mechanism<sup>46</sup> while 60 mV/decade indicates that a chemical rearrangement step limits catalytic activity.<sup>49</sup> The Tafel slopes for these  $[\text{Mo}_3\text{S}_{13}]^{2-}$  catalysts were determined to be approximately 40-60 mV/decade, values which are commonly observed for molybdenum sulfide catalysts.<sup>22</sup> Interestingly, the Tafel slopes are different for each electrode, indicating that the mechanism of catalysis or conductivity may be changing as a function of support material.<sup>50</sup> The Tafel slope of the  $[\text{Mo}_3\text{S}_{13}]^{2-}/\text{GC}$  and  $[\text{Mo}_3\text{S}_{13}]^{2-}/\text{Ag}$  are 45 mV/decade and 48 mV/decade, respectively, while the Tafel slopes of the  $[\text{Mo}_3\text{S}_{13}]^{2-}/\text{Au}$  and  $[\text{Mo}_3\text{S}_{13}]^{2-}/\text{Cu}$  are 58 mV/decade and 66 mV/decade, respectively. An average of Tafel slopes of three replicates for each catalyst-support system is presented in Table S2. Further investigation is necessary to elucidate the specific mechanistic impacts of the catalyst-support interactions.

In order to deconvolute the effects of support interactions from catalyst loading and obtain a more intrinsic measure of activity, we calculate a current density per Mo atom (Fig. 2c), by using ICP-MS to determine the number of Mo atoms on the electrode (Table S1). The trend in geometric current density is conserved after this normalization though the magnitude of the activity difference between  $[\text{Mo}_3\text{S}_{13}]^{2-}/\text{Au}$  and  $[\text{Mo}_3\text{S}_{13}]^{2-}/\text{Cu}$  decreases. The activity differences among the electrodes provide evidence for the effects of catalyst-support interactions in enhancing HER activity. We note though, that the cluster-normalized activity dependence is a strong function of catalyst loading. As shown in Fig. S5, the magnitude of the substrate effects decreases with increasing loading. While the sulfur atoms have been identified as the active site of many molybdenum sulfide materials, the low catalyst loadings here make it difficult to quantify sulfur using ICP-MS due to overlap with  $\text{O}_2$ .

The normalized current density profiles can be expressed as a turnover frequency (TOF) per Mo atom (details available in supporting information), a common metric in the field of molybdenum sulfide catalysis.<sup>22</sup> The TOF of an HER catalysts corresponds to the number  $\text{H}_2$  molecules produced per second, and in this case, per Mo atom. Fig. 2d shows the TOF per Mo atom for each electrode. At -200 mV vs. RHE, a potential where the reported TOFs of all electrodes are influenced only by catalytic activity and not by non-faradic current or mass transport limitations, the TOFs of  $[\text{Mo}_3\text{S}_{13}]^{2-}$  on Au, Ag, GC, and Cu supports respectively are 0.47, 0.27, 0.15, 0.045  $\text{H}_2 \text{ s}^{-1}$  per Mo atom. The approximately one order of magnitude difference between the TOF of the Au and Cu supported  $[\text{Mo}_3\text{S}_{13}]^{2-}$  clusters is strong evidence of a catalyst-support interaction that has a large effect on catalytic activity.

### Understanding trends in catalytic activity

Density functional theory (DFT) was employed to calculate differential hydrogen absorption free energies ( $\Delta G_{\text{H}}$ ) in order to understand the role of support effects in tuning the activity of  $[\text{Mo}_3\text{S}_{13}]^{2-}$  catalysts.  $\Delta G_{\text{H}}$  has previously been used as a descriptor to successfully describe the HER activity trends in a variety of systems including pure transition metals, transition metal sulfides, phosphides, and carbides.<sup>36, 51-53</sup> The periodic computational unit-cells consisted of a single  $\text{Mo}_3\text{S}_{13}$  cluster on top of the fcc(111) surface or a single graphene surface. The  $\Delta G_{\text{H}}$  was determined in the same way as in previous studies.<sup>36, 41</sup> The structures and further details about the computational methodology are provided in the Supporting Information (Table S4).

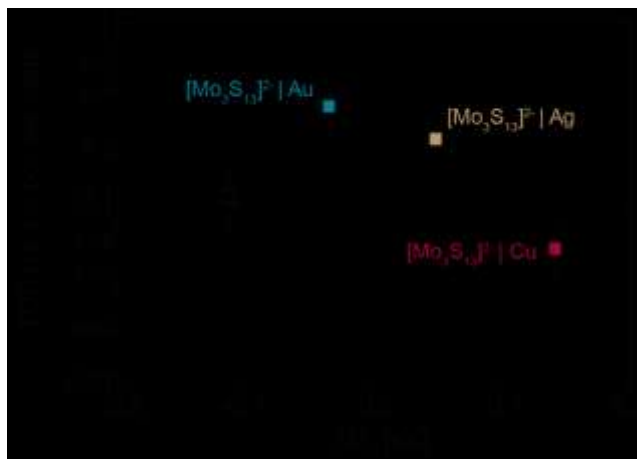


Figure 3. Activity for the HER showing the average TOF from Fig. 2d at  $\eta = 200$  mV as a function of  $\Delta G_{\text{H}}$ . Each point represents the average of three different samples and the error bars display the standard deviation. The  $\Delta G_{\text{H}}$  for each sample was calculated using density functional theory. The plotted points show a volcano type relationship with the  $[\text{Mo}_3\text{S}_{13}]^{2-}/\text{Au}$  electrode as the most active. The dashed lines are drawn as a guide for the eyes.

Fig. 3 plots the TOF per Mo atom of all electrodes measured at 200 mV overpotential versus the calculated  $\Delta G_{\text{H}}$ . The resulting plot suggests a volcano-like trend in activity which qualitatively resembles the HER activity volcano for pure transition metals with the peak near  $\Delta G_{\text{H}} = 0$  eV.<sup>51</sup> The data points presented on the plot correspond to an average of three replicates for each electrode. Though more material systems are required to confirm the presence of the volcano relationship, the four points in Fig. 3 show that the activity tends toward a maximum around  $\Delta G_{\text{H}} = 0$  eV as shown by the qualitatively drawn dashed lines. The reported activities are a conservative lower bound as they take into account all Mo atoms present on the electrode after electrochemical testing. Post electrochemical characterization XPS analysis (Fig. S2) shows that there is likely some oxidation of the clusters into  $\text{MoO}_x$ . However, it is also possible that the  $[\text{Mo}_3\text{S}_{13}]^{2-}$  catalysts oxidize upon air exposure after electrochemical testing. Fig. S6 shows that the volcano trend still holds even after correcting the TOF for the ratio of  $\text{MoS}_x:\text{MoO}_x$  as determined by XPS. The  $[\text{Mo}_3\text{S}_{13}]^{2-}/\text{Au}$  electrode is the most active followed by the  $[\text{Mo}_3\text{S}_{13}]^{2-}$  on Ag, GC, and Cu with average TOFs of 0.35, 0.21, 0.11, and 0.05  $\text{H}_2 \text{ s}^{-1}$  per Mo atom, respectively at  $\eta = 200$  mV. These results



show that it is important to consider the choice of support when testing novel materials for catalytic activity and that engineering catalyst-support interactions can provide a potential pathway for tuning the  $\Delta G_{\text{H}}$  of highly active catalysts to further improve their activity.

Herein we have demonstrated the ability to tune the activity of highly active  $[\text{Mo}_3\text{S}_{13}]^{2-}$  cluster HER catalysts by changing the electrode support material. We show that combining theory and experiment to plot the supported catalysts' TOF versus the computed  $\Delta G_{\text{H}}$  gives a volcano plot activity relationship which is qualitatively similar to other HER volcano plots presented in the literature.

It is important to note that catalyst-support effects only apply to the first few monolayers of a catalyst due to a rapidly diminishing electronic influence as a function of distance from the support. Moving forward it will be important to leverage appropriate synthesis techniques to engineer electrodes which pair optimal high surface area supports with HER catalysts that benefit most from the catalyst-support interactions.

## EXPERIMENTAL AND COMPUTATIONAL METHODS

**Information on experimental methods regarding the synthesis of  $[\text{Mo}_3\text{S}_{13}]^{2-}$  nanoclusters electrodes, electrode preparation, electrochemical characterization, and physical characterization are provided in the Supporting Information. Periodic plane-wave DFT calculations with ultra-soft pseudopotentials were performed using the Quantum ESPRESSO code.<sup>54</sup> Further details are provided in the Supporting Information.**

## ASSOCIATED CONTENT

Supporting information including experimental and computational methods, additional characterization, and explanation of turnover frequency calculations is provided online. This material is available free of charge via the Internet at <http://pubs.acs.org>.

## AUTHOR INFORMATION

### Corresponding Author

\*Thomas F. Jaramillo

Department of Chemical Engineering, Stanford University  
443 Via Ortega, Stanford, California 94305, United States  
[jaramillo@stanford.edu](mailto:jaramillo@stanford.edu)

### Author Contributions

The manuscript was written through contributions of all authors. T.R. Hellstern and J. Kibsgaard contributed equally to this work.

### Funding Sources

Funding provided through DOE Hydrogen Production Research and Development, contract number DE-EE006670. Funding also provided by the U.S. Department of Energy (DOE), Office of Basic Energy Sciences for the SUNCAT Center for Interface Science and Catalysis and the Villum Foundation V-SUSTAIN grant 9455 to the Villum Center for the Science of Sustainable Fuels and Chemicals. This study was also funded through NSF project (Award Number CBET-1433442) competitively selected under the solicitation "NSF 14-15: NSF/DOE Partnership on Advanced Frontiers in Renewable

Hydrogen Fuel Production via Solar Water Splitting Technologies", which was cosponsored by the National Science Foundation, Division of Chemical, Bioengineering, Environmental, and Transport Systems (CBET) and the U.S. Department of Energy, Office of Energy Efficiency and Renewable Energy, Fuel Cell Technologies Office

## ACKNOWLEDGMENT

T.R.H. and C.T. acknowledge support from the National Science Foundation Graduate Research Fellowship Program. J.K., F.A.-P. acknowledge financial support from the U.S. Department of Energy (DOE), Office of Basic Energy Sciences for the SUNCAT Center for Interface Science and Catalysis. J.K. further acknowledge financial support from the Villum Foundation V-SUSTAIN grant 9455 to the Villum Center for the Science of Sustainable Fuels and Chemicals. Electrode synthesis was performed in part at the Stanford Nanofabrication Facility (SNF) Physical characterization was performed at the Stanford Nano Shared Facility (SNSF). L.A.K. acknowledges the NSF (Award Number CBET-1433442)

## REFERENCES

- (1) Häussinger, P.; Lohmüller, R.; Watson, A. M., Hydrogen, 6. Uses. In *Ullmann's Encyclopedia of Industrial Chemistry*, Wiley-VCH Verlag GmbH & Co. KGaA: 2000.
- (2) Badwal, S. P.; Giddey, S.; Munnings, C. *Wiley Interdiscip. Rev.: Energy Environ.* **2013**, 2, 473-487.
- (3) Kim, J. W.; Boo, K. J.; Cho, J. H.; Moon, I., 1 - Key challenges in the development of an infrastructure for hydrogen production, delivery, storage and use. In *Advances in Hydrogen Production, Storage and Distribution*, Basile, A.; Iulianelli, A., Eds. Woodhead Publishing: 2014; pp 3-31.
- (4) Bak, T.; Nowotny, J.; Rekas, M.; Sorrell, C. C. *Int. J. Hydrogen Energy* **2002**, 27, 991-1022.
- (5) Pinaud, B. A.; Benck, J. D.; Seitz, L. C.; Forman, A. J.; Chen, Z. B.; Deutsch, T. G.; James, B. D.; Baum, K. N.; Baum, G. N.; Ardo, S.; Wang, H. L.; Miller, E.; Jaramillo, T. F. *Energy Environ. Sci.* **2013**, 6, 1983-2002.
- (6) Walter, M. G.; Warren, E. L.; McKone, J. R.; Boettcher, S. W.; Mi, Q. X.; Santori, E. A.; Lewis, N. S. *Chem. Rev.* **2010**, 110, 6446-6473.
- (7) McCrory, C. C. L.; Jung, S.; Ferrer, I. M.; Chatman, S.; Peters, J. C.; Jaramillo, T. F. *J. Am. Chem. Soc.* **2015**.
- (8) Vesborg, P. C. K.; Seger, B.; Chorkendorff, I. *J. Phys. Chem. Lett.* **2015**, 951-957.
- (9) Vesborg, P. C. K.; Jaramillo, T. F. *RSC Adv.* **2012**, 2, 7933-7947.
- (10) McKone, J. R.; Warren, E. L.; Bierman, M. J.; Boettcher, S. W.; Brunschwig, B. S.; Lewis, N. S.; Gray, H. B. *Energy Environ. Sci.* **2011**, 4, 3573.
- (11) McKone, J. R.; Sadtler, B. F.; Werlang, C. A.; Lewis, N. S.; Gray, H. B. *ACS Catal.* **2013**, 3, 166-169.
- (12) Vrubel, H.; Hu, X. L. *Angew. Chem. Int. Ed.* **2012**, 51, 12703-12706.
- (13) Jaramillo, T. F.; Jorgensen, K. P.; Bonde, J.; Nielsen, J. H.; Hørch, S.; Chorkendorff, I. *Science* **2007**, 317, 100-102.
- (14) McEnaney, J. M.; Crompton, J. C.; Callejas, J. F.; Popczun, E. J.; Read, C. G.; Lewis, N. S.; Schaak, R. E. *Chem. Commun.* **2014**, 50, 11026-11028.
- (15) Popczun, E. J.; McKone, J. R.; Read, C. G.; Biacchi, A. J.; Wilttrout, A. M.; Lewis, N. S.; Schaak, R. E. *J. Am. Chem. Soc.* **2013**, 135, 9267-9270.
- (16) Popczun, E. J.; Read, C. G.; Roske, C. W.; Lewis, N. S.; Schaak, R. E. *Angew. Chem.* **2014**, 126, 5531-5534.
- (17) Hellstern, T. R.; Benck, J. D.; Kibsgaard, J.; Hahn, C.; Jaramillo, T. F. *Adv. Energy Mater.* **2016**, 6.
- (18) Gao, M. R.; Liang, J. X.; Zheng, Y. R.; Xu, Y. F.; Jiang, J.; Gao, Q.; Li, J.; Yu, S. H. *Nat. Comm.* **2015**, 6.

- (19) Seh, Z. W.; Kibsgaard, J.; Dickens, C. F.; Chorkendorff, I. B.; Norskov, J. K.; Jaramillo, T. F. *Science* **2017**, 355, 146-+.
- (20) Chen, W. F.; Sasaki, K.; Ma, C.; Frenkel, A. I.; Marinkovic, N.; Muckerman, J. T.; Zhu, Y. M.; Adzic, R. R. *Angew. Chem. Int. Ed.* **2012**, 51, 6131-6135.
- (21) Shi, Y. M.; Zhang, B. *Chem. Soc. Rev.* **2016**, 45, 1529-1541.
- (22) Benck, J. D.; Hellstern, T. R.; Kibsgaard, J.; Chakthranont, P.; Jaramillo, T. F. *ACS Catal.* **2014**, 4, 3957-3971.
- (23) Kibsgaard, J.; Chen, Z. B.; Reinecke, B. N.; Jaramillo, T. F. *Nat. Mater.* **2012**, 11, 963-969.
- (24) Li, Y. G.; Wang, H. L.; Xie, L. M.; Liang, Y. Y.; Hong, G. S.; Dai, H. J. *J. Am. Chem. Soc.* **2011**, 133, 7296-7299.
- (25) Benck, J. D.; Chen, Z. B.; Kuritzky, L. Y.; Forman, A. J.; Jaramillo, T. F. *ACS Catal.* **2012**, 2, 1916-1923.
- (26) Merki, D.; Vrubel, H.; Rovelli, L.; Fierro, S.; Hu, X. L. *Chem. Sci.* **2012**, 3, 2515-2525.
- (27) Wang, H. T.; Lu, Z. Y.; Kong, D. S.; Sun, J.; Hymel, T. M.; Cui, Y. *ACS Nano* **2014**, 8, 4940-4947.
- (28) Voiry, D.; Salehi, M.; Silva, R.; Fujita, T.; Chen, M. W.; Asefa, T.; Shenoy, V. B.; Eda, G.; Chhowalla, M. *Nano Lett.* **2013**, 13, 6222-6227.
- (29) Jaramillo, T. F.; Bonde, J.; Zhang, J. D.; Ooi, B. L.; Andersson, K.; Ulstrup, J.; Chorkendorff, I. *J. Phys. Chem. C* **2008**, 112, 17492-17498.
- (30) Karunadasa, H. I.; Montalvo, E.; Sun, Y. J.; Majda, M.; Long, J. R.; Chang, C. J. *Science* **2012**, 335, 698-702.
- (31) Kibsgaard, J.; Jaramillo, T. F.; Besenbacher, F. *Nat. Chem.* **2014**, 6, 248-253.
- (32) Nørskov, J. K.; Bligaard, T.; Logadottir, A.; Kitchin, J.; Chen, J. G.; Pandelov, S.; Stimming, U. *J. Electrochem. Soc.* **2005**, 152, J23-J26.
- (33) Skúlason, E.; Tripkovic, V.; Björketun, M. E.; Gudmundsdóttir, S.; Karlberg, G.; Rossmeisl, J.; Bligaard, T.; Jónsson, H.; Nørskov, J. K. *J. Phys. Chem. C* **2010**, 114, 18182-18197.
- (34) Hinnemann, B.; Moses, P. G.; Bonde, J.; Jørgensen, K. P.; Nielsen, J. H.; Hørch, S.; Chorkendorff, I.; Nørskov, J. K. *J. Am. Chem. Soc.* **2005**, 127, 5308-5309.
- (35) Greeley, J.; Jaramillo, T. F.; Bonde, J.; Chorkendorff, I.; Nørskov, J. K. *Nat. Mater.* **2006**, 5, 909-913.
- (36) Kibsgaard, J.; Tsai, C.; Chan, K.; Benck, J. D.; Nørskov, J. K.; Abild-Pedersen, F.; Jaramillo, T. F. *Energy Environ. Sci.* **2015**, 8, 3022-3029.
- (37) Li, H.; Tsai, C.; Koh, A. L.; Cai, L.; Contryman, A. W.; Fraga, A. H.; Zhao, J.; Han, H. S.; Manoharan, H. C.; Abild-Pedersen, F.; Nørskov, J. K.; Zheng, X. *Nat. Mater.* **2016**, 15, 48-53.
- (38) Dai, X. P.; Du, K. L.; Li, Z. Z.; Liu, M. Z.; Ma, Y. D.; Sun, H.; Zhang, X.; Yang, Y. *ACS Appl. Mater. Interfaces* **2015**, 7, 27242-27253.
- (39) Wang, H. T.; Tsai, C.; Kong, D. S.; Chan, K. R.; Abild-Pedersen, F.; Nørskov, J.; Cui, Y. *Nano Res.* **2015**, 8, 566-575.
- (40) Tsai, C.; Chan, K. R.; Nørskov, J. K.; Abild-Pedersen, F. *Catal. Sci. Technol.* **2015**, 5, 246-253.
- (41) Tsai, C.; Abild-Pedersen, F.; Nørskov, J. K. *Nano Lett.* **2014**, 14, 1381-1387.
- (42) Muller, A.; Sarkar, S.; Bhattacharyya, R. G.; Pohl, S.; Dartmann, M. *Angew. Chem., Int. Ed. Engl.* **1978**, 17, 535-535.
- (43) Muller, A.; Jostes, R.; Jaegermann, W.; Bhattacharyya, R. G. *Inorg. Chim. Acta* **1980**, 41, 259-263.
- (44) Buckley, A. N.; Woods, R. *Colloids Surf., A* **1995**, 104, 295-305.
- (45) Mikhlin, Y.; Likhatski, M.; Tomashevich, Y.; Romanchenko, A.; Erenburg, S.; Trubina, S. *J. Electron Spectrosc. Relat. Phenom.* **2010**, 177, 24-29.
- (46) Harrington, D. A.; Conway, B. E. *Electrochim. Acta* **1987**, 32, 1703-1712.
- (47) Conway, B. E.; Tilak, B. V. *Electrochim. Acta* **2002**, 47, 3571-3594.
- (48) Bai, L.; Harrington, D. A.; Conway, B. E. *Electrochim. Acta* **1987**, 32, 1713-1731.
- (49) Kodintsev, I. M.; Trasatti, S. *Electrochim. Acta* **1994**, 39, 1803-1808.
- (50) Vrubel, H.; Moehl, T.; Gratzel, M.; Hu, X. *Chem. Commun.* **2013**, 49, 8985-8987.
- (51) Greeley, J.; Nørskov, J. K.; Kibler, L. A.; El-Aziz, A. M.; Kolb, D. M. *ChemPhysChem* **2006**, 7, 1032-1035.
- (52) Hinnemann, B.; Moses, P. G.; Bonde, J.; Jørgensen, K. P.; Nielsen, J. H.; Hørch, S.; Chorkendorff, I.; Nørskov, J. K. *J. Am. Chem. Soc.* **2005**, 127, 5308-5309.
- (53) Michalsky, R.; Zhang, Y. J.; Peterson, A. A. *ACS Catal.* **2014**, 4, 1274-1278.
- (54) Giannozzi, P.; Baroni, S.; Bonini, N.; Calandra, M.; Car, R.; Cavazzoni, C.; Ceresoli, D.; Chiarotti, G. L.; Cococcioni, M.; Dabo, I. *J. Phys.: Condens. Matter* **2009**, 21, 395502.

## TOC Figure

